Data-Driven Multi-Scale Modeling and Optimization for Elastic Properties of Cubic Microstructures

M. Hasan [1], Y. Mao [2], K. Choudhary [3,4], F. Tavazza [3],
A. Choudhary [2], A. Agrawal [2], P. Acar[1*]

July 15, 2022

1. Virginia Tech, Blacksburg, VA, United States
2. Northwestern University, Evanston, IL, United States
3. National Institute of Standards and Technology, Gaithersburg, MD, United States
4. Theiss Research, La Jolla, CA, United States
*Corresponding author: Pınar Acar (pacar@vt.edu)

Abstract

The present work addresses gradient-based and machine learning (ML)-driven design optimization methods to enhance homogenized linear and non-linear properties of cubic microstructures. The study computes the homogenized properties as a function of underlying microstructures by linking atomistic-scale and meso-scale models. Here, the microstructure is represented by the Orientation Distribution Function (ODF) that determines the volume densities of crystallographic orientations. The homogenized property matrix in meso-scale is computed using the single-crystal property values that are obtained by Density Functional Theory (DFT) calculations. The optimum microstructure designs are validated with the available data in the literature. The single-crystal designs, as expected, are found to provide the extreme values of the linear properties, while the optimum values of the non-linear properties could be provided by single or polycrystalline microstructures. However, polycrystalline designs are advantageous over single crystals in terms of better manufacturability. With this in mind, an ML-based sampling algorithm is presented to identify top optimum polycrystal solutions for both linear and non-linear properties without compromising the optimum property values. Moreover, an inverse optimization strategy is presented to design microstructures for prescribed values of homogenized properties, such as the stiffness constant (C_{11}) and in-plane Young's modulus (E_{11}). The applications are presented for Aluminium (Al), Nickel (Ni), and Silicon (Si) microstructures.

Background & Summary

The field of multi-scale material design aims to identify the material features that provide optimum properties for specific engineering applications, including problems in aerospace, automotive, and navy [1, 2, 3]. The throughout effort of the last decade to design theoretical tools for optimizing material microstructures is named as 'microstructure-sensitive design for performance optimization' (MSDPO) [4, 5]. The main advantage of this approach is its ability to create a design space of all possible values of the desired parameters, which allows the designer to select the optimum solution of the design parameter(s) for a particular engineering problem [6, 7]. Additionally, this optimum property solution can be mapped back to the corresponding microstructure space which will help determine the optimum manufacturing route of the material [8]. The microstructure that provides the maximum value of the desired parameter (e.g. stiffness constant, C_{11}) may not be an optimum solution for another parameter (e.g. C_{12}). However, this challenge also creates an opportunity for materials design to achieve a prescribed material property for a particular application by tailoring the microstructures [9, 10].

Different approaches have been taken by the researchers to obtain the optimum material properties with the microstructure-sensitive design. Acharjee et al. [11] and Ganapathysubramanian et al. [12] applied proper orthogonal decomposition (POD) and method of snapshots in Rodrigues space to develop the reduced-order model representation of the microstructural orientations in a polycrystalline material. This strategy was able to save significant computational time. The material design was performed for a compliant beam microstructure by Adams et al. [13] through generating a spectral representation of the Orientation Distribution Function (ODF), which defines the design variables for the polycrystalline material [14, 15]. A similar approach was adopted by Kalidindi et al. [16] for designing a thin plate with a circular hole in the center to maximize the uniaxial load-carrying capacity of the plate without plastic deformation. The microstructure-sensitive design method was applied to the hexagonal closed packed (HCP) microstructures by Fast et al. [17] to obtain the design space of elasto-plastic properties of a cantilever beam that is made of alpha Titanium. Other optimization studies on materials design include the finite element analysis [18] and graph-based method [19] as reported in the literature to improve mechanical properties of polycrystalline materials.

More recently, a linear programming algorithm was used to find out the microstructural textures that lead to optimum volume-averaged properties using the idea of building a reduced-order design space, called the property closure [20, 21, 22]. The optimization techniques can also be used within this reduced space to calculate the desired properties by designing the microstructural texture. The applications of this approach were performed by Acar et al. [21] including the example of finding the best microstructure design of an airframe panel for obtaining the maximum buckling temperature. This process was extended to find the maximum yield strength of the Galfenol alloy while the constraints for the vibration tuning were considered [22]. In both cases, the property closures

of several homogenized stiffness parameters were generated and utilized for the solution.
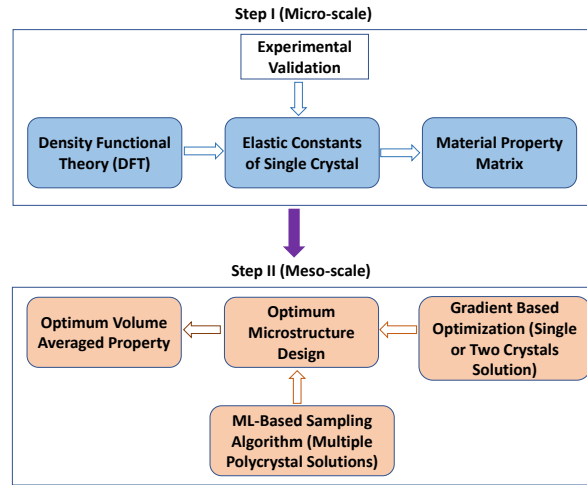

Figure 1: Block diagram of this study. Step I is performed at micro-scale to get the volume averaged optimized property at meso-scale level in Step II.

Density Functional Theory (DFT) has been proven as a powerful tool to understand micro-scale material behavior [23, 24]. DFT uses the first principle calculation to determine the material properties at the atomic/electronic level. Though it requires a significant amount of calculations, new-generation computational resources may improve its computational time efficiency and reliability [25, 26]. On the other hand, machine learning (ML) has become a popular and robust tool in science and engineering, including the problems for material design and discovery [27, 28, 29, 30, 31].

The present work will mainly build upon the previous work for the microstructure design by extending the study to three cubical materials (Al, Ni, and Si) from a total of 4721 materials in the JARVIS-DFT database [32, 33]. Our goal is to optimize the meso-scale material properties by linking the atomistic scale simulation (DFT) and the microstructure model. In particular, gradient-based and ML-based optimization algorithms are applied to find the optimum (maximum and minimum) stiffness constant (C_{11}) and Young's modulus (E_{11}) values along with the corresponding microstructures defined in terms of the ODFs. Moreover, the ML-based sampling algorithm is able to reduce the dimensions of the ODF space and generate numerous solutions (top optimum designs) that are close to the optimum microstructure solution. Finally, the results from these approaches will be compared and validated with the previous works from the literature for both linear (C_{11}) and non-linear (E_{11}) properties. Figure 1 summarizes this study in a block diagram which consists of two steps. Step I comprises of determining the elastic tensor values of the cubic materials by utilizing the DFT calculations. With these tensor values, the property

matrix of each material is generated and used in Step II. The homogenized material properties (e.g. C_{11} and E_{11}) are optimized in Step II using gradient-based optimization and the ML-based sampling algorithms. As expected, the homogenized linear property (C_{11}) has a single-crystal optimum solution while the non-linear property (E_{11}) still has a sharp texture optimum solution but it is a polycrystal with two non-zero independent ODFs. The presented ML technique is shown to find both optimum designs that involve the single-crystal solution of C_{11} and the sharp texture polycrystalline solution of E_{11}, as well as identifying other top optimum designs for both properties. The ML solution is verified against the gradient-based optimization solution (Sequential Quadratic Programming (SQP)) for different optimum microstructure designs and may be extended to more challenging multi-scale design optimization problems (e.g. optimization of crystal plasticity properties) in the future by taking advantage of its computational time efficiency. Moreover, the optimum texture is determined using SQP for a given value of E_{11} (near to the maximum value) which corresponds to a polycrystal solution. Additionally, the ML-based approach is also used to generate multiple polycrystalline textures for E_{11}. These findings are significant as the polycrystalline microstructures are known to be advantageous over single crystal designs in terms of cost, performance, ease of manufacturing, homogeneity, and good control over composition [34], while the single crystals have direct use areas where the anisotropic elastic properties are required [35]. The presented microstructure formulation can be applied to model the materials that have different crystallographic structures (i.e., hexagonal close-packed, face-centered cubic, body-centered cubic). Similarly, the optimization approach will also be applicable to the design of different microstructures in the future by extending the presented methodology. The arrangement of this article is as follows: The modeling section comprises atomistic-scale modeling (DFT), microstructure modeling (ODF), gradient-based optimization model, and the ML-based optimization model. Next, the numerical results are presented and discussed for both linear and non-linear properties of Al, Ni, and Si. Finally, the summary of the study along with the future works to be accomplished are narrated in the conclusion.

Background for Modeling

Four different models have been developed in this study. In the first step, the single-crystal material property values are determined by DFT calculations. The microstructures of the sample materials are modeled using the ODF approach. Later on, a multi-scale optimization model is developed and solved using gradient-based optimization and ML to find the extreme C_{11} and E_{11} values and the corresponding microstructures. The details of these models are discussed in the following sections.

Density Functional Theory

Density functional theory (DFT) calculations were carried out with Vienna Ab-initio Simulation Package (VASP) and the projector-augmented wave (PAW) method [36, 37]. Please note that commercial software is identified to specify procedures. Such identification does not imply a recommendation by the National Institute of Standards and Technology. The structure relaxation with OptB88vdW functional [38] was obtained with 10^{-8} eV energy tolerance and 0.001 eV/Å force-convergence criteria. The elastic tensor is determined by performing six finite distortions of the lattice and deriving the elastic constants from the strain-stress relationship. Further details about the DFT elastic-constant database can be found in Ref [32].

Microstructure Modeling

A polycrystalline material consists of several crystals having different crystallographic orientations that define the microstructural texture. The individual orientations of the crystals are represented by the angle-axis parameterization technique by Rodrigues. This method follows a different approach of representing crystal orientations in comparison to the Euler angles [39, 40]. The interested readers are referred to the study by Kumar et al. [41] for detailed information on Rodrigues parameterization of microstructural solution spaces. In this work, the microstructure is described using the ODF, which defines the volume density of each unique crystal orientation in the microstructure. A local finite element discretization scheme is applied along with the Rodrigues parametrization to compute the meso-scale features. The definition of the ODF, in terms of the volume densities of the crystals, requires the implementation of the normalization constraint that is expressed by the following equation:

$$\int_R A(r,t)\,dv = 1 \tag{1}$$

Homogenization aims to compute the volume-averaged properties of the polycrystalline microstructures as a function of the single-crystal properties. For example, using the Taylor estimation [42], the volume-averaged elastic properties C^{avg} of homogeneous polycrystalline materials can be obtained from the following equation:

$$C^{avg} = <C> \tag{2}$$

where, C is the stiffness tensor of each crystal and $<.>$ is the symbol of averaging. Similarly, if any property of a single crystal $\chi(r)$, which is dependent on the crystal orientation, is known, then the homogenized polycrystal property $<\chi>$ can be determined by performing the averaging over the ODF. Mathematically, the expression is:

$$<\chi> = \int_R \chi(r)A(r,t)\,dv \tag{3}$$

As mentioned earlier, the crystal orientation is represented by the Rodrigues parameterization, which is obtained from the scaling of the axis of rotation, n,
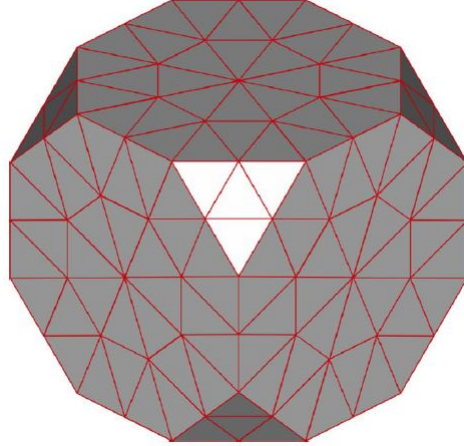
Figure 2: Finite element discretization of the orientation space

that is expressed in terms of the orientation, r, and angle of rotation, θ, as: $n = r/tan(\theta/2)$. In Eq. (3), $\chi(r)$ represents the single-crystal material properties that are obtained from the DFT simulations (stored in JARVIS). The computation of the homogenized microstructure properties using the single-crystal data is explained next.

Computation of Homogenized Properties using Single-Crystal Property Data Obtained from DFT Simulations: The homogenized (volume-averaged) properties of the microstructures are obtained using the given expression in Eq. (3). Here, the integration for the homogenized properties is performed over the fundamental domain by considering the rotation of the crystals, R. Given the Rodrigues orientation vector, r, the rotation, R can be obtained with the following expression:

$$R = \frac{1}{1 + r \cdot r}(I(1 - r \cdot r) + 2(r \otimes r + I \times r)) \qquad (4)$$

Any polycrystal property obtained using Eqs. (3) and (4) can be shown in the linear form by this parameterization [20]. The finite element discretization of the microstructural orientation space is exhibited in Fig. 2. Here, each independent nodal point of the finite element mesh represents a unique ODF value for the associated crystal. The matrix representation of Eq. (3) can be written as follows:

$$\begin{aligned}
< \chi > &= \int_R \chi(r)A(r,t)\,dv \\
&= \sum_{n=1}^{N_{elem}} \sum_{n=1}^{N_{int}} \chi(r_m)A(r_m)\omega_m|J_n|\frac{1}{(1 + r_m.r_m)^2}
\end{aligned} \qquad (5)$$

where, N_{elem} is the number of elements of the finite element mesh with N_{int} integration points in each element, and $A(r_m)$ is the ODF value at the mth integration point with global coordinate r_m of the nth element. $|J_n|$ is the Jacobian matrix of the nth element and ω_m is the integration weight of the mth integration point. The Rodrigues parameterization metric is given by:

$$\frac{1}{(1 + r_m.r_m)^2}$$

The expression in Eq. (5) is given in terms of the nodal point values, while it can also be derived in terms of the properties defined at the integration points: $< \chi > = P^{int^T} A^{int}$, which is a linear form in terms of the ODF at integration points:

$$P^{int} = \chi(r_i)\omega_i|J_i|\frac{1}{(1 + r_i.r_i)^2} \quad \text{and} \quad A^{int} = A(r_i)$$

where, i=1,2,........$N_{int} \times N_{elem}$.

When the symmetry arising from the cubic crystalline system is considered, the number of independent nodal points decreases. Let A be the vector of ODF values at the independent nodes that are obtained from the integration point values, A^{int}, using the tetrahedral finite element definition. Next, the properties can simply be represented as $< \chi > = P^T A$ in terms of the independent nodal point ODF values. The nodal point property matrix, P^T, can also be computed from P^{int^T}. Here, the meso-scale stiffness tensor can be computed using the microstructure homogenization expression (for example, $C_{11} = P_{11}^T A$, where P_{11} is the property matrix of the single-crystal values for C_{11}). The Young's modulus (E_{11}), on the other hand, is inversely related to the stiffness as it is given by $E_{11} = \frac{1}{S_{11}}$, where $S_{11} = S(1,1)$ while S is the compliance matrix defined as $S = C^{-1}$. Therefore, it is called a non-linear property. Similarly, the normalization constraint of Eq. (1) can be written in the linear form as $q^T A = 1$. Finally, the ODF must satisfy the following non-negativity condition ($A \geq 0$).

Gradient-Based Optimization

Two separate optimization problems are defined for the multi-scale model. One of them is to find the optimum microstructures that maximize and minimize the C_{11} and E_{11} values. The second problem is to obtain the microstructure design that provides a prescribed value of E_{11}. In both cases, the Sequential Quadratic Programming (SQP) algorithm is applied to solve the optimization problem. Table 1 shows the mathematical definitions of these optimization problems.

The ODF solutions of the optimization problem in Table 1 need to satisfy two design constraints, i.e., the volume normalization constraint and the non-negativity of the ODFs.

max and min C_{11} and E_{11} subject to: $q^T A = 1$ $A \geq 0$	min (E_{11}- design E_{11} value) subject to: $q^T A = 1$ $A \geq 0$

Table 1: Summary of the optimization problems to maximize and minimize C_{11} and E_{11} values and design microstructures for a prescribed E_{11} value.

ML-based Optimization Model

An ML-based optimization method is used to find multiple polycrystal solutions in the microstructure space. The applied method is similar to the approach of Paul et al. [27]. The framework of the ML-based optimization method is showed in Figure 3. There are three main steps in this approach.
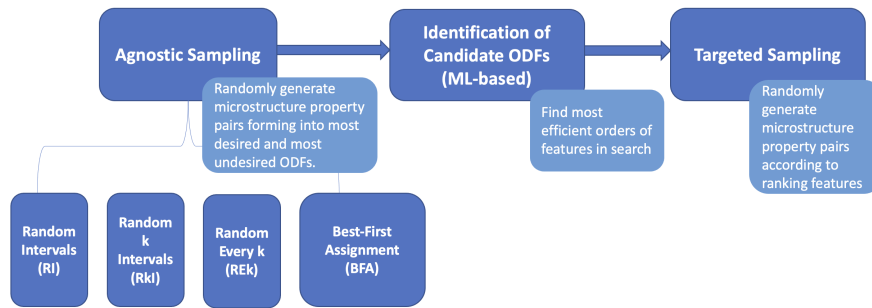

Figure 3: Framework of ML-based optimization method.

In the first step, agnostic sampling methods are used to randomly generate microstructure property pairs: the most desirable set of ODFs and the most undesirable set of ODFs. Compared to Paul et al.'s problem [27], our problem has no additional constraints, so four sampling algorithms, Random Intervals, Random k Intervals, Random Every k, and Best-First Assignment [43] are used here. In the experiments, each of the four algorithms generate around 1 million valid ODFs, thereby a total of 4 million ODFs.

The second step is the identification of candidate ODF dimensions using ML-based methods. The purpose here is to evaluate ODF dimensions which are more important for generating optimum solutions. The top 10% and bottom 10% data of ODFs in terms of the desired design objective are selected, and labeled as "High" and "Low". Then, random forest-based [44] models are constructed to predict the output using the ODF dimensions as features. The feature importance from these models can thus help to rank the ODF dimensions in the order of their importance.

The third step is targeted sampling. In this step, we proceed to the second iteration of sampling only on a subset of ODF dimensions that are more important in providing near-optimum solutions, instead of sampling across all dimensions. Firstly, only m dimensions that are advantageous in providing near-optimum solutions are selected. Further, k dimensions from the m dimensions

are randomly selected for sampling. After that, we iterate k from $\{3, 4, 5, 6, 7\}$ when m is equal to 10, and from $\{6, 7, 8, 9, 10\}$ when m is equal to 20. For each k and m parameters pairs, N iterations of sampling are performed to generate optimum solutions. Finally, all solutions obtained from different parameters are aggregated. It was observed in our experiments that as we increase the value of the parameter N, it increases the time of sampling, which in turn leads to better results. The value of N is 1 million for the experiments in this study.

Results and Discussions

The optimization of the meso-scale stiffness constant, C_{11}, and the in-plane Young's modulus, E_{11}, is performed for the three cubic materials by gradient-based and ML-based algorithms. In both cases, the material property matrix is computed using the DFT data in JARVIS. The optimum results obtained from two optimization methods are compared to the literature data for the same parameters. The gradient-based SQP algorithm can identify the local optimum solution for the microstructure design. However, the ML technique can produce multiple optimum solutions that will be discussed in this section.

Optimization of a Linear Property (C_{11})

The single-crystal microstructure, which is intrinsically anisotropic, provides the maximum and minimum values of C_{11} in the $<111>$ and $<100>$ directions, respectively [45, 46]. The gradient-based algorithm of this study is also able to find the single-crystal ODFs for the maximum and minimum C_{11}. However, the ML-based optimization obtains top optimum solutions corresponding to polycrystalline microstructures. To the best of the authors' knowledge, there is no experimental study that is performed for finding the meso-scale maximum or minimum C_{11} value. It is also difficult to manufacture single-crystal materials. Therefore, we have chosen the experimental values of C_{11} from the literature without labeling them maximum or minimum to validate the numerical results. Table 2 shows the optimum values for C_{11} using gradient-based optimization and ML methods, and their comparison with the available experimental data from the previous studies [47, 48] for the three example materials.

Material	Gradient-based Optimization		Machine Learning		C_{11} from the literature [47, 48]
	C_{11}^{max}	C_{11}^{min}	C_{11}^{max}	C_{11}^{min}	
Al	122.8104	107.202	122.8102	107.2456	112
Ni	346.2944	268.0388	346.293	268.2173	268
Si	184.9062	156.5225	184.906	156.5787	168

Table 2: Comparison of maximum and minimum of the stiffness constant (C_{11}) values obtained from gradient-based optimization and ML along with the validation with the literature data (unit of C_{11} is GPa)

Table 2 shows that both optimization algorithms are providing almost equal C_{11}^{max} and C_{11}^{min} values and the experimental C_{11} value lies between them for

all the three example materials. However, the significance of the ML-based technique is that it can generate multiple polycrystalline textures with C_{11} values that are close to the optimum value of C_{11}. This is advantageous for manufacturing purposes. Figure 4 depicts the optimum microstructures that provide C_{11}^{max} for Al, Ni, and Si generated by both optimization techniques.
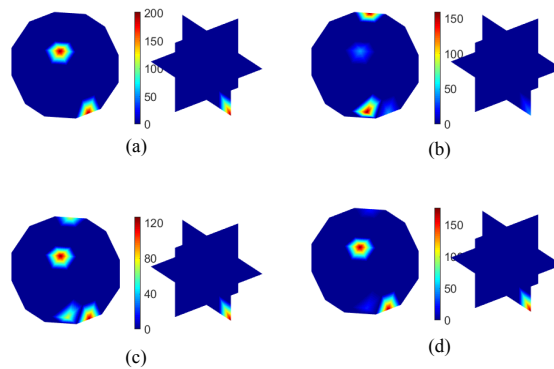

Figure 4: Optimum microstructures (ODFs) in the orientation space for (a) C_{11}^{max} of Al by gradient-based optimization and C_{11}^{max} of (b) Al (c) Ni and (d) Si by ML approach.

Optimization of a Non-Linear Property (E_{11})

The selected non-linear property is the in-plane Young's modulus value (E_{11}). Accordingly, E_{11}^{max} and E_{11}^{min} are calculated for Al, Ni, and Si by gradient-based optimization and ML methods. In this case, unlike the homogenized linear properties, there is no guarantee that the single-crystal microstructure will yield extreme values of the non-linear parameter [6]. This is also verified through our observation in the present study as a sharp polycrystalline texture with two non-zero ODF values is found to be the optimum solution by both design methods. The optimized E_{11}^{max} value is used for comparison with the literature [49, 50] as the maximization of the in-plane Young's modulus (E_{11}) is naturally a more important design problem for improved elasticity. Table 3 reports the optimum values of E_{11} from both approaches and their validation with the available data from the previous studies for the three example materials.

It is evident from Table 3 that the E_{11}^{max} values obtained from the gradient-based optimization algorithm and ML are almost identical, where the maximum difference for all cases is below 1 GPa. The E_{11}^{max} values for Al and Si are used from Cantwell et al. [49] where the authors estimated the in-plane Young's modulus as a function of crystallographic directions for microelectromechanical systems (MEMS). On the other hand, the Ni data was used from the study by Ju et al. [50] which modeled the nanoindentation of a Ni surface at different

Material	Gradient-based Optimization		Machine Learning		E_{11}^{max} from the literature [49, 50]	Error (%)
	E_{11}^{max}	E_{11}^{min}	E_{11}^{max}	E_{11}^{min}		
Al	77.7468	48.2523	77.7462	48.5039	72.3	7.3
Ni	277.5323	140.2831	277.5119	141.2446	288	3.9
Si	170.0734	127.84	170.0647	128.0674	172	0.5

Table 3: Comparison of maximum and minimum in-plane Young's modulus values (E_{11}) obtained from gradient-based optimization and ML along with the validation with the literature data (unit of E_{11} is GPa)

crystal orientations using molecular dynamic (MD) simulations to approximate the maximum E_{11}. The outcomes of the presented optimization approach also provide similar E_{11}^{max} for these materials. The percentage of errors for Al, Ni, and Si are 7.3%, 3.9%, and 0.5%, respectively. We anticipate that these errors arise from the microstructural uncertainties and the differences in modeling assumptions. For example, the two-crystal optimum solution of the present work is a sharp texture design that is substantially difficult to process. Therefore, there could be differences between the mathematical optimum solutions and processed textures. Another possible error source can be the epistemic uncertainties related to the computational methods (e.g. modeling assumptions, convergence, errors).

The next objective objective of this study is to design the microstructure for a prescribed value of E_{11} using gradient-based optimization (see Table 1). Therefore, we have considered three different values of E_{11} (close to the E_{11}^{max} value) for the example materials. For instance, the E_{11} values of Al are determined as 75 GPa, 76.5 GPa, and 77 GPa where the E_{11}^{max} of Al is 77.75 GPa. Similarly, the chosen values for Ni are 270 GPa, 273 GPa, and 275 GPa while its maximum value for E_{11} is 277.5 GPa. These values for Si are 165 GPa, 167.5
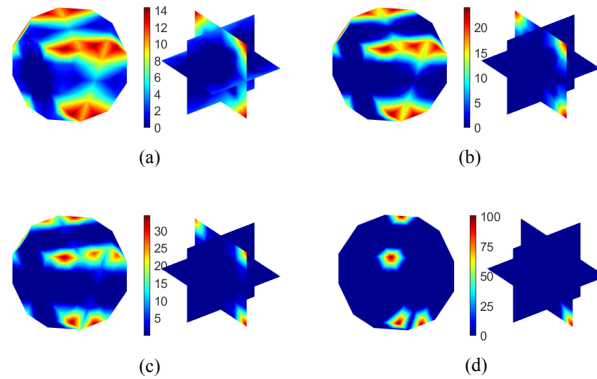

Figure 5: Optimized microstructures (ODFs) in the orientation space with (a) E_{11}=75 GPa (b) E_{11}=76.5 GPa (c) E_{11}=77 GPa and (d) E_{11}^{max}=77.5 GPa of Al.
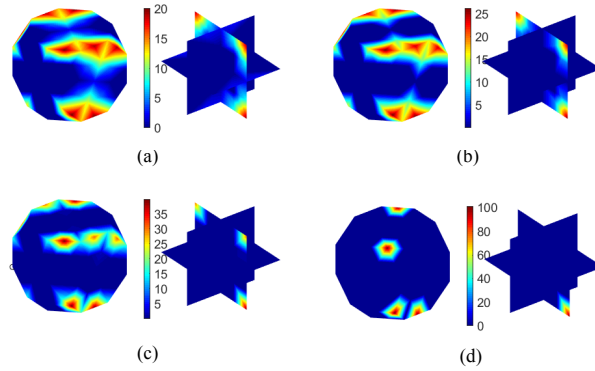
Figure 6: Optimized microstructures (ODFs) in the orientation space with (a) E_{11}=270 GPa (b) E_{11}=273 GPa (c) E_{11}=275 GPa and (d) E_{11}^{max}=277.53 GPa of Ni.

GPa, and 169 GPa where E_{11}^{max} is 170.06 GPa. For all three microstructures, the results exhibit that the ODFs converge to the optimum sharp texture design (two-crystal solution) as E_{11} approaches its maximum value.
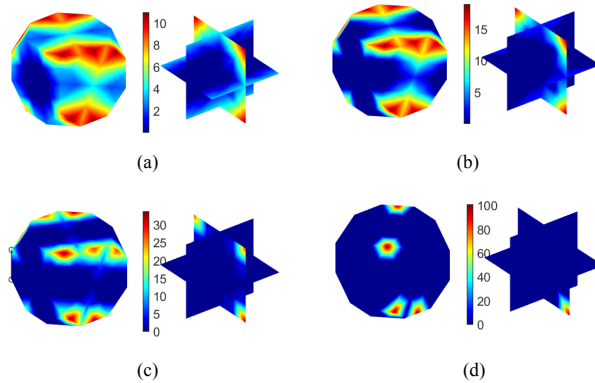

Figure 7: Optimized microstructures (ODFs) in the orientation space with (a) E_{11}=165 GPa (b) E_{11}=167.5 GPa (c) E_{11}=169 GPa and (d) E_{11}^{max}=170.06 GPa of Si.

This outcome is also visible from Figs. 5-7. For example, in Fig. 5, the microstructures (ODFs) of Al are plotted in the Rodrigues orientation space for the three prescribed E_{11} values and the maximum E_{11} value. Figure 5(a) represents the microstructure with E_{11} value of 75 GPa, which demonstrates a smooth polycrystalline texture. The texture becomes sharper as the E_{11} value increases, e.g. E_{11} of 76.5 GPa (Fig. 5(b)) and E_{11} of 77 GPa (Fig. 5(c)).

Finally, the optimum two-crystal texture providing the E_{11}^{max}) value of 77.75 GPa is depicted in Fig. 5(d) which is obtained from both optimization techniques. The optimum microstructure designs for Ni and Si, in Fig. 6 and Fig. 7, respectively, follow the same trend. This result underlines the two unique orientations for cubic microstructures that lead to maximum in-plane Young's modulus. The presented technique for inverse design can be applied to all polycrystalline microstructures to achieve the prescribed values of the homogenized material properties. For manufacturing purposes, the ML approach can be integrated into the design framework to identify the top optimum polycrystalline microstructure designs.

Optimization Results for ML

The optimum values of C_{11} and E_{11} obtained by gradient-based optimization and ML are compared in Tables 2 and 3, respectively as the results of the proposed ML method are comparable to the conventional optimization results. The optimum designs of the gradient-based method are a single-crystal for C_{11} and a two-crystal texture for E_{11}. On the contrary, the ML method provides multiple solutions with more than two strictly non-zero ODF dimensions owing to its parameter setting to improve the manufacturability of the microstructures. The number of the top optimum designs (top 0.01%, 0.1%, 0.5%, and 1% designs) identified by the ML model are shown in Table 4 and 5 for C_{11} and E_{11}, respectively.

Material		within 0.01%	within 0.1%	within 0.5%	within 1%
Al	C_{11}^{min}	0	8	130	232
	C_{11}^{max}	103	210	409	584
Ni	C_{11}^{min}	0	7	90	151
	C_{11}^{max}	72	210	405	429
Si	C_{11}^{min}	0	12	125	230
	C_{11}^{max}	102	222	405	485

Table 4: Number of polycrystal solutions for C_{11} obtained by ML-based method within 0.01%, 0.1%, 0.5%, 1% of the optimum solutions.

Material		within 0.01%	within 0.1%	within 0.5%	within 1%
Al	E_{11}^{min}	0	0	0	2
	E_{11}^{max}	3	48	701	2431
Ni	E_{11}^{min}	0	0	0	1
	E_{11}^{max}	1	50	549	1936
Si	E_{11}^{min}	0	0	5	12
	E_{11}^{max}	8	130	1943	2676

Table 5: Number of polycrystal solutions for E_{11} obtained by ML-based method within 0.01%, 0.1%, 0.5%, 1% of the optimum solutions.

As represented by Tables 4 and 5, the method successfully finds multiple near-optimum polycrystal solutions for all three materials. The near-optimum

solutions correspond to different microstructure designs having the same or similar values for the stiffness constant and Young's modulus. In the case of C_{11}^{max} optimization, 103, 72, and 102 solutions can be discovered for Al, Ni, and Si respectively within a neighborhood of 10^{-4} from the optimum solution. Furthermore, 584, 429 and 485 solutions within a neighborhood of 10^{-2} are discovered respectively for C_{11}^{max} problem. Similarly, for C_{11}^{min} calculation, 232, 151, and 230 solutions in a neighborhood of 10^{-2}, for Al, Ni, and Si respectively, are identified.

On the other hand, 3, 1, and 8 solutions can be discovered for Al, Ni, and Si respectively for E_{11}^{max} determination within a neighborhood of 10^{-4} from the optimum solution. Furthermore, 2431, 1936 and 2676 solutions within a neighborhood of 10^{-2} are suggested respectively for E_{11}^{max} of those materials. Next, for E_{11}^{min} problem, 2, 1, and 12 solutions in a neighborhood of 10^{-2}, for Al, Ni, and Si respectively, are identified.

It is critical to obtain multiple near-optimum solutions because traditional low-cost manufacturing processes can only generate a limited set of microstructures. Multiple near-optimum solutions can accelerate materials development efforts by increasing the variability of optimum designs and, thus, improve the efficiency of manufacturing immensely. Therefore, given the ability of the ML-based sampling algorithm to identify promising microstructure design spaces which can then be rigorously searched to discover multiple polycrystal solutions, it can be applied as a useful tool for the challenging multi-scale design optimization problem (e.g. optimization of crystal plasticity properties).

Conclusions

Two optimization algorithms are developed in this study to determine the optimum values of linear (C_{11}) and non-linear (E_{11}) properties and corresponding microstructures for three cubic materials: Al, Ni, and Si. First, the homogenized material properties of the microstructures are computed by linking the DFT calculations with the ODF-based microstructure model. The first design approach utilizes the gradient-based optimization that provides single-crystal optimum microstructures for the extreme values of C_{11} and two-crystal designs for E_{11}. The second design approach is based on ML-based optimization that is able to produce numerous polycrystalline microstructures without compromising the optimum values of the homogenized properties. For example, 2431, 1936, and 2676 optimum microstructure solutions are suggested within 1% of E_{11}^{max} value of Al, Ni, and Si, respectively. This outcome is significant to accelerate the manufacturing of materials by increasing the variability of optimum design solutions. The numerical results for the optimum microstructures are validated for different materials using the available data in the literature. In the future, this approach can be extended to other crystalline structures, such as hexagonal, monoclinic, trigonal, and tetragonal microstructures, and to more complex multi-scale design problems, such as the design of microstructures under large deformations using crystal plasticity simulations.

Acknowledgements

Author contributions

MH and PA conducted the research on microstructure modeling with ODF. KC and FT conducted the research on DFT. YM, AC, and AA conducted the machine learning research. All authors contributed to the manuscript preparation.

Competing interests

The authors declare no conflict of interest.

References

[1] Yu Liu, M Steven Greene, Wei Chen, Dmitriy A Dikin, and Wing Kam Liu. Computational microstructure characterization and reconstruction for stochastic multiscale material design. *Computer-Aided Design*, 45(1):65–76, 2013.

[2] Bassam Mohammed, Taejoon Park, Farhang Pourboghrat, Jun Hu, Rasoul Esmaeilpour, and Fadi Abu-Farha. Multiscale crystal plasticity modeling of multiphase advanced high strength steel. *International Journal of Solids and Structures*, 151:57–75, 2018.

[3] Mark F Horstemeyer. *Integrated Computational Materials Engineering (ICME) for metals: using multiscale modeling to invigorate engineering design with science*. John Wiley & Sons, 2012.

[4] Brent L Adams, Surya Kalidindi, and David T Fullwood. *Microstructure sensitive design for performance optimization*. Butterworth-Heinemann, 2012.

[5] Oliver K Johnson and Christian Kurniawan. An efficient algorithm for generating diverse microstructure sets and delineating properties closures. *Acta Materialia*, 147:313–321, 2018.

[6] Pinar Acar. A new sampling approach for the multi-scale design of metallic materials. *Journal of Mechanical Design*, 142(8), 2020.

[7] Surya R Kalidindi, Massimiliano Binci, David Fullwood, and Brent L Adams. Elastic properties closures using second-order homogenization theories: case studies in composites of two isotropic constituents. *Acta Materialia*, 54(11):3117–3126, 2006.

[8] David T Fullwood, Stephen R Niezgoda, Brent L Adams, and Surya R Kalidindi. Microstructure sensitive design for performance optimization. *Progress in Materials Science*, 55(6):477–562, 2010.

[9] Ole Sigmund. Tailoring materials with prescribed elastic properties. *Mechanics of Materials*, 20(4):351–368, 1995.

[10] Hongyi Xu, Yang Li, Catherine Brinson, and Wei Chen. A descriptor-based design methodology for developing heterogeneous microstructural materials system. *Journal of Mechanical Design*, 136(5), 2014.

[11] Swagato Acharjee and Nicholas Zabaras. A proper orthogonal decomposition approach to microstructure model reduction in rodrigues space with applications to optimal control of microstructure-sensitive properties. *Acta Materialia*, 51(18):5627–5646, 2003.

[12] Shankar Ganapathysubramanian and Nicholas Zabaras. Design across length scales: a reduced-order model of polycrystal plasticity for the control of microstructure-sensitive material properties. *Computer Methods in Applied Mechanics and Engineering*, 193(45-47):5017–5034, 2004.

[13] Brent L Adams, A Henrie, B Henrie, M Lyon, SR Kalidindi, and H Garmestani. Microstructure-sensitive design of a compliant beam. *Journal of the Mechanics and Physics of Solids*, 49(8):1639–1663, 2001.

[14] Olaf Engler and Valerie Randle. *Introduction to texture analysis: macrotexture, microtexture, and orientation mapping.* CRC press, 2009.

[15] U Fred Kocks, Carlos Norberto Tomé, and H-R Wenk. *Texture and anisotropy: preferred orientations in polycrystals and their effect on materials properties.* Cambridge university press, 1998.

[16] Surya R Kalidindi, Joshua R Houskamp, Mark Lyons, and Brent L Adams. Microstructure sensitive design of an orthotropic plate subjected to tensile load. *International Journal of Plasticity*, 20(8-9):1561–1575, 2004.

[17] Tony Fast, Marko Knezevic, and Surya R Kalidindi. Application of microstructure sensitive design to structural components produced from hexagonal polycrystalline metals. *Computational Materials Science*, 43(2):374–383, 2008.

[18] Xiu-Juan Zhang, Ke-Zhang Chen, and Xin-An Feng. Optimization of material properties needed for material design of components made of multi-heterogeneous materials. *Materials & design*, 25(5):369–378, 2004.

[19] Pengfei Du, Adrian Zebrowski, Jaroslaw Zola, Baskar Ganapathysubramanian, and Olga Wodo. Microstructure design using graphs. *npj Computational Materials*, 4(1):1–7, 2018.

[20] Veera Sundararaghavan and Nicholas Zabaras. Linear analysis of texture–property relationships using process-based representations of rodrigues space. *Acta materialia*, 55(5):1573–1587, 2007.

[21] Pinar Acar and Veera Sundararaghavan. Utilization of a linear solver for multiscale design and optimization of microstructures. *AIAA Journal*, pages 1751–1759, 2016.

[22] Pinar Acar and Veera Sundararaghavan. Linear solution scheme for microstructure design with process constraints. *AIAA Journal*, pages 4022–4031, 2016.

[23] Peter Rogl, Raimund Podloucky, and Walter Wolf. Dft calculations: a powerful tool for materials design, 2014.

[24] Jürgen Hafner, Christopher Wolverton, and Gerbrand Ceder. Toward computational materials design: the impact of density functional theory on materials research. *MRS bulletin*, 31(9):659–668, 2006.

[25] Jörg Neugebauer and Tilmann Hickel. Density functional theory in materials science. *Wiley Interdisciplinary Reviews: Computational Molecular Science*, 3(5):438–448, 2013.

[26] Gabriel R Schleder, Antonio CM Padilha, Carlos Mera Acosta, Marcio Costa, and Adalberto Fazzio. From dft to machine learning: recent approaches to materials science–a review. *Journal of Physics: Materials*, 2(3):032001, 2019.

[27] Arindam Paul, Pinar Acar, Wei-keng Liao, Alok Choudhary, Veera Sundararaghavan, and Ankit Agrawal. Microstructure optimization with constrained design objectives using machine learning-based feedback-aware data-generation. *Computational Materials Science*, 160:334–351, 2019.

[28] Jaimyun Jung, Jae Ik Yoon, Hyung Keun Park, Jin You Kim, and Hyoung Seop Kim. An efficient machine learning approach to establish structure-property linkages. *Computational Materials Science*, 156:17–25, 2019.

[29] Dipendra Jha, Logan Ward, Arindam Paul, Wei-keng Liao, Alok Choudhary, Chris Wolverton, and Ankit Agrawal. Elemnet: Deep learning the chemistry of materials from only elemental composition. *Scientific reports*, 8(1):1–13, 2018.

[30] Rampi Ramprasad, Rohit Batra, Ghanshyam Pilania, Arun Mannodi-Kanakkithodi, and Chiho Kim. Machine learning in materials informatics: recent applications and prospects. *npj Computational Materials*, 3(1):1–13, 2017.

[31] Pei Liu, Haiyou Huang, Stoichko Antonov, Cheng Wen, Dezhen Xue, Houwen Chen, Longfei Li, Qiang Feng, Toshihiro Omori, and Yanjing Su. Machine learning assisted design of γ'-strengthened co-base superalloys with multi-performance optimization. *npj Computational Materials*, 6(1):1–9, 2020.

[32] Kamal Choudhary, Gowoon Cheon, Evan Reed, and Francesca Tavazza. Elastic properties of bulk and low-dimensional materials using van der waals density functional. *Physical Review B*, 98(1):014107, 2018.

[33] Kamal Choudhary, Kevin F Garrity, Andrew CE Reid, Brian DeCost, Adam J Biacchi, Angela R Hight Walker, Zachary Trautt, Jason Hattrick-Simpers, A Gilad Kusne, Andrea Centrone, et al. The joint automated repository for various integrated simulations (jarvis) for data-driven materials design. *npj Computational Materials*, 6(1):1–13, 2020.

[34] Laurent Mezeix and David J Green. Comparison of the mechanical properties of single crystal and polycrystalline yttrium aluminum garnet. *International journal of applied ceramic technology*, 3(2):166–176, 2006.

[35] Xinpeng Du and Ji-Cheng Zhao. Facile measurement of single-crystal elastic constants from polycrystalline samples. *npj Computational Materials*, 3(1):1–8, 2017.

[36] Georg Kresse and Jürgen Furthmüller. Efficient iterative schemes for ab initio total-energy calculations using a plane-wave basis set. *Physical review B*, 54(16):11169, 1996.

[37] Georg Kresse and Jürgen Furthmüller. Efficiency of ab-initio total energy calculations for metals and semiconductors using a plane-wave basis set. *Computational materials science*, 6(1):15–50, 1996.

[38] Jiří Klimeš, David R Bowler, and Angelos Michaelides. Chemical accuracy for the van der waals density functional. *Journal of Physics: Condensed Matter*, 22(2):022201, 2009.

[39] H-J Bunge. *Texture analysis in materials science: mathematical methods.* Elsevier, 2013.

[40] Hans Rudolf Wenk. *Preferred orientation in deformed metal and rocks: an introduction to modern texture analysis.* Elsevier, 2016.

[41] A Kumar and PR Dawson. Computational modeling of fcc deformation textures over rodrigues' space. *Acta Materialia*, 48(10):2719–2736, 2000.

[42] Geoffrey Ingram Taylor. Plastic strain in metals. *J. Inst. Metals*, 62:307–324, 1938.

[43] Ruoqian Liu, Abhishek Kumar, Zhengzhang Chen, Ankit Agrawal, Veera Sundararaghavan, and Alok Choudhary. A predictive machine learning approach for microstructure optimization and materials design. *Scientific reports*, 5(1):1–12, 2015.

[44] Andy Liaw, Matthew Wiener, et al. Classification and regression by randomforest. *R news*, 2(3):18–22, 2002.

[45] Klosek, Vincent. Crystallographic textures. *EPJ Web Conf.*, 155:00005, 2017.

[46] Karsten Kunze, Thomas Etter, Jürgen Grässlin, and Valery Shklover. Texture, anisotropy in microstructure and mechanical properties of in738lc alloy processed by selective laser melting (slm). *Materials Science and Engineering: A*, 620:213–222, 2015.

[47] RFS Hearmon. The elastic constants of anisotropic materials—ii. *Advances in Physics*, 5(19):323–382, 1956.

[48] P Haldipur, FJ Margetan, and RB Thompson. Estimation of single-crystal elastic constants from ultrasonic measurements on polycrystalline specimens. In *AIP Conference Proceedings*, volume 700, pages 1061–1068. American Institute of Physics, 2004.

[49] Patrick R Cantwell, Hojin Kim, Matthew M Schneider, Hao-Han Hsu, Dimitrios Peroulis, Eric A Stach, and Alejandro Strachan. Estimating the in-plane young's modulus of polycrystalline films in mems. *Journal of microelectromechanical systems*, 21(4):840–849, 2012.

[50] S-P Ju, C-T Wang, C-H Chien, JC Huang, and S-R Jian. The nanoindentation responses of nickel surfaces with different crystal orientations. *Molecular Simulation*, 33(11):905–917, 2007.